frontiers | Frontiers in Earth Science

TYPE Original Research
PUBLISHED 03 November 2022
DOI 10.3389/feart.2022.1012286

OPEN ACCESS

EDITED BY
Stanislaw Mazur,
Institute of Geological Sciences, Polish Academy of Sciences, Poland

REVIEWED BY
Chris Green,
University of Leeds, United Kingdom
Alexandra Guy,
Czech Geological Survey, Czechia

*CORRESPONDENCE
Darharta Dahrin,
darharta@gmail.com

SPECIALTY SECTION
This article was submitted to Structural Geology and Tectonics, a section of the journal Frontiers in Earth Science

RECEIVED 05 August 2022
ACCEPTED 25 October 2022
PUBLISHED 03 November 2022

CITATION
Dahrin D, Amir H, Suryanata PB, Bijaksana S, Fajar SJ, Ibrahim K, Harlianti U, Arisbaya I, Pebrian MQ, Rahman AA and Kasendri A (2022), Subsurface structures of Sianok Segment in the GSF (Great Sumatran Fault) inferred from magnetic and gravity modeling.
Front. Earth Sci. 10:1012286.
doi: 10.3389/feart.2022.1012286

Subsurface structures of Sianok Segment in the GSF (Great Sumatran Fault) inferred from magnetic and gravity modeling

Darharta Dahrin[1]*, Harman Amir[2], Putu Billy Suryanata[1], Satria Bijaksana[1], Silvia Jannatul Fajar[1], Khalil Ibrahim[1], Ulvienin Harlianti[1], Ilham Arisbaya[1,3], Mutiara Qalbi Pebrian[1], Adinda Aisyah Rahman[1] and Adibbian Kasendri[1]

[1]Faculty of Mining and Petroleum, Institut Teknologi Bandung, Bandung, Indonesia, [2]Faculty of Mathematics and Natural Sciences, Universitas Negeri Padang, Padang, Indonesia, [3]Research Center for Geological Disaster, National Research and Innovation Agency (BRIN), Bandung, Indonesia

Among the 19 segments of the Great Sumatran Fault (GSF), the Sianok segment is unique due to its proximity to active volcanoes as well as to the sizable Maninjau Caldera. Located next to the Sumani to its southeast, the Sianok segment also passes through a relatively densely populated area. To identify potential disasters in the future, it is imperative to understand the subsurface structures of the Sianok segment. In this study, ground magnetic measurements were conducted, and the data were combined with the Bouguer anomaly map. Hand samples were also collected and measured for magnetic susceptibility and density. The values were later used as initial parameters for modeling. Joint forward modeling of magnetic and gravity was then used in the modeling stage as well as in the interpretation stage. Subsurface models of 20 km in depth were then formulated based on the magnetic and gravity data. The models show shallow magma chambers beneath Maninjau Caldera, Mount Marapi, and Mount Singgalang-Tandikat. The models confirm that exposed and unexposed Permian metamorphic rocks are commonly distributed in the Sianok segment. The thickness of volcanic deposits such as tuff and andesites in the Sianok segment were found to be sizable, ranging from 1 km for tuff to 3.5 km for andesites of the Maninjau Caldera.

KEYWORDS

Great Sumatran Fault, Sianok, 2D modeling, magnetic, gravity, Indonesia

Introduction

The Sianok segment is one of the segments in the GSF located in West Sumatra Province. Like the Sumani segment, the Sianok segment is an area that needs to be studied thoroughly because of the large human population living in the area. However, unlike the Sumani segment, which is dominated by a pull-apart basin, the Sianok segment is dominated by volcanic activity. The geomorphology of the Sianok segment is

characterized by the presence of towering volcanoes and the second largest caldera lake on the island of Sumatra after Lake Toba. To analyze the seismic hazard potential of earthquakes along the GSF, published studies have focused on field observations of surface ruptures (Daryono et al., 2012; Daryono and Tohari, 2016), paleoearthquakes (Bellier et al., 1997), active fault mapping (Sieh and Natawidjaja, 2000; Weller et al., 2012; Natawidjaja et al., 2017; Muksin et al., 2019), fault slip rates (Bellier and Sebrier, 1995; Genrich et al., 2000; Prawirodirdjo et al., 2000; Ito et al., 2012; Bradley et al., 2017; Natawidjaja et al., 2017; Tong et al., 2018), and source characteristics of ruptures (Duquesnoy et al., 1996; Prawirodirdjo et al., 2000; Ito et al., 2016; Gunawan et al., 2018).

The results of the subsurface structure study by Amir et al. (2021), based on combined magnetic and gravity data, are important for understanding the earthquake mechanism in the Sumani segment, which is one of the seismically active GSF segments that is located on the border of the Sianok segment. Why is it necessary to study the Sianok subsurface? The occurrence of the 1926 and 2007 doublet earthquakes depended on the presence of tectonic stress, the rigidity of the crust, and the geological structure. Tectonic stress can be identified based on earthquake analysis and surface deformation based on GPS data. On the other hand, the subsurface structure provides the presence of rock types related to the rigidity and geometry/distribution of subsurface rocks related to the geological structure. As reported by Amir et al. (2021), subsurface intrusion may be related to earthquake events. Natural disasters depend on the rate of deformation of the ground surface, which depends on the subsurface structure. Subsurface structures can explain how the GSF is related to volcanic activity where the Marapi complex is located (Figure 1A,B). Volcanic activity certainly depends on subsurface structures, such as the presence of magma chambers and volcanic rock structures.

A combination of gravity and magnetic methods is commonly used to identify subsurface geological structures (see Zubaidah et al., 2014; Jiang et al., 2017; Araffa et al., 2018; Amir et al., 2021). The combination of gravitational and magnetic data is often used to overcome the problem of lack of data or the presence of non-uniqueness in the solution of the inversion process (Hinze et al., 2012). Zubaidah et al. (2014) integrated gravitational and magnetic methods in their study on Lombok Island, Indonesia and succeeded in identifying two active normal faults (in the quarter) and a magmatic arc associated with subduction areas. This identification helps scientists to better understand the occurrence of the 1988 Lombok earthquake. Furthermore, the combination of magnetic and gravitational methods carried out by Jiang et al. (2017) in the Western Pacific Ocean succeeded in identifying offshore basins and their geodynamic models that are useful in understanding the evolution of the Western Pacific. A study using the same method has also been carried out by Araffa et al. (2018) in the Sinai Peninsula and identified the main tectonic deformation sites in the study area. Recently, Amir et al. (2021) also conducted magnetic and gravitational studies in the Sumani Segment of the Great Sumatran Fault (GSF) and identified the presence of unexposed intrusive bodies in the study area, including under Lake Singkarak. The results of the study by Amir et al. (2021) are important for understanding the earthquake mechanism in the Sumani segment, which is one of the seismically active GSF segments.

Models of subsurface structures help scientists not only to identify earthquake risks in a particular area but also provide insight into the interplay between fault development and volcanism. This insight is important as several segments of the GSF are associated with volcanism. In this study, models of subsurface structures near the Sianok segment were constructed from ground magnetic data combined with regional gravity data from previous surveys by Buyung et al. (1992a), Buyung et al. (1992b).

Tectonic setting

Sumatra, the third largest island in Indonesia, was formed in the Paleozoic to early Mesozoic because of the collision between Paleozoic crustal blocks brought from the Gondwana continent and the eastern edge of Sundaland. Sumatran bedrock is thought to be composed of sedimentary and volcanic rocks that have undergone partial deformation and metamorphism (Barber, 2000; Barber and Crow, 2005; Setiawan et al., 2017). The GSF that covers the entire island of Sumatra is a 1650-km-long dextral strike-slip fault zone that accommodates part of the oblique convergence of the subduction between the Indo-Australian and Eurasian plates (Hamilton, 1979; Bellier et al., 1997). This subduction is responsible for megathrust earthquakes such as the 2004 Sumatra-Andaman earthquake (Ammon et al., 2005).

McCarthy and Elders (1997) argued that the strike-slip mode of GSF was initiated in the mid-Miocene. According to Wesnousky (1988), strike-slip faults such as the GSF consist of segments, and at the segment boundaries are related to geological offsets; the strength along the fault plane is a function of all geological offsets along the fault. Based on the geomorphic expression of an active fault and on the geological map, Sieh and Natawidjaja (2000) divided the GSF into 19 segments. Four of these 19 segments (from NW to SE, Sumpur, Sianok, Sumani, and Suliti) are in the West Sumatra Province. However, other scientists, like Burton and Hall (2014), divided the GSF based on seismic clustering into 16 segments. The slip rate of these nineteen segments varies between 5 and 27 mm/yr (Sieh and Natawidjaja, 2000), averaging 14 and 15 mm/year (Bradley et al., 2017). Furthermore, the Sianok segment's minimum slip rate is estimated to be 14.5 ± 0.5 mm/yr (Bradley et al., 2017). Based on GPS studies, Prawirodirdjo et al. (2000) and Genrich et al. (2000)

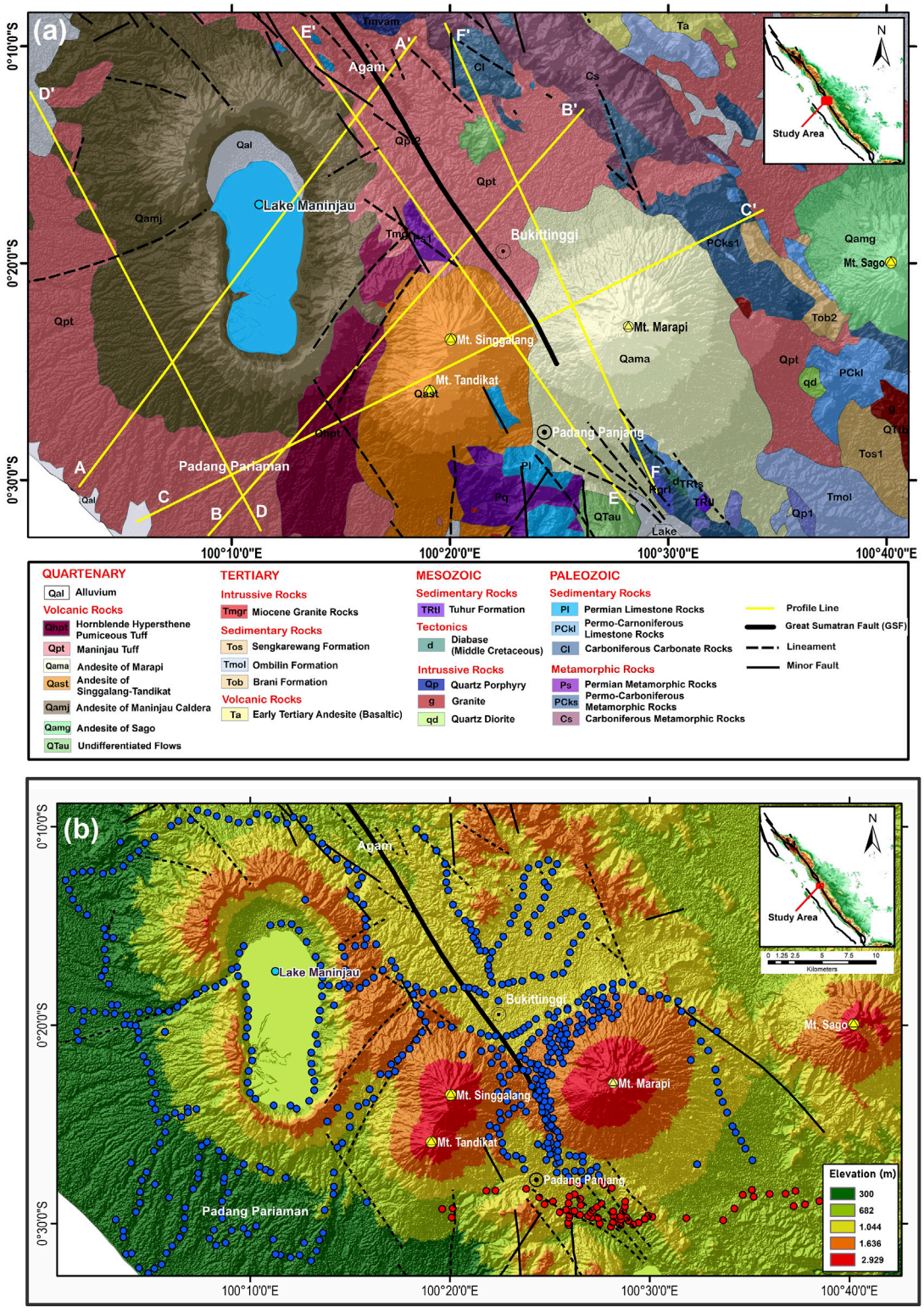

FIGURE 1
(A) Geological map of the Sianok segment of GSF showing the fault line, lithologies in the study area (modified from Kastowo et al., 1996 and by Silitonga and Kastowo, 1995), and the six profiles (A-A′, B-B′, C-C′, D-D′, E-E′, and F-F′) shown as thick yellow lines; **(B)** topographic map of the Sianok segment, including magnetic survey point locations along existing roads and dirt roads. Certain areas, especially near the volcanoes, are not accessible due to their terrain. Blue circles are new survey points, while red survey points were from Amir et al. (2021).

determined that the slip rate of the Sianok segment is 23 mm/yr with a locking depth of 24 km.

Although not as active as the Sumani segment, which borders on the southeast, the Sianok segment is also classified as seismically active. Doublet earthquakes occurred in 1926 and 2007 to the northwest of Lake Singkarak at the border between the Sumani segment and the Sianok segment (Nakano et al., 2010; Daryono et al., 2012; Salman et al., 2020). In the 1926 doublet earthquake, the first earthquake occurred with a magnitude of Ms 6.5 in the Sumani segment and was followed 3 hours later by a second earthquake with a magnitude of Ms 6.75 in the Sianok segment (Daryono et al., 2012). In the 2007 doublet earthquake, the first earthquake occurred with a magnitude of Ms 6.4 in the Sumani segment at a depth of 22 km and was followed 2 hours later by a second earthquake with a magnitude of Ms 6.3 in the Sianok segment at a depth of 22.5 km (Daryono et al., 2012; Salman et al., 2020).

Apart from the extensive fault system, GSF is also home to extensive volcanic activity, recorded to be the highest in arcs in terms of magmatic productivity (Acocella, 2014). The Toba Caldera Complex is the largest magmatic system in the GSF. The effects of local structures on volcanism in the GSF are not well understood (Acocella, 2014). Acocella et al. (2018) identified that some of the volcanoes are likely controlled by GSF structures, while others are probably and possibly linked to GSF. Posavec et al. (1973) named seven volcanic centers (from north to south) as follows: Marapi, Talang, Kerintji, Hulumajang, Pandan, Kaba, and Dempo after their most striking or active members. At each volcanic center, there is a series of active and dormant volcanoes that stretch in the E-W direction. The line connecting the volcanoes forms an angle of about 70 in the direction of the GSF (Posavec et al., 1973). The Marapi Centre, located in the Sianok segment, is one of the more active centers (Figure 1A). The last known eruption of Mount Marapi was in 2018 (Smithsonian Institution, 2022). Based on geothermobarometry and seismic receiver function methods, Nurfiani et al. (2021) identified two magma chambers beneath Mount Marapi. According to Acocella et al. (2018), the Marapi Center is possibly linked to GSF. The Marapi Centre features two great active cones, namely Marapi and Singgalang-Tandikat, that rise to about 3000 m near Bukittinggi. The other important feature of the Marapi Center is Lake Maninjau, a 16 by 7 km caldera with a maximum depth of 169 m (Wills et al., 2021). According to Posavec et al. (1973), this caldera is the product of three major eruptions that generated extensive tuff cover in the surrounding area. The extent of tuff cover could be appreciated in the Sianok canyon in Bukittinggi. Based on petrographic analyses of transparent and non-transparent white pumice from the Maninjau caldera-forming eruption, Suhendro (2021) identified that the shallow magma chamber of the Maninjau Caldera is located at a depth of about 6 km.

As shown in Figure 1A, the Sianok segment is composed of various rock units ranging from Permian metamorphic (limestone) rocks to Quaternary sedimentary and volcanic rocks (see Silitonga and Kastowo, 1995; Kastowo et al., 1996). As described earlier by Amir et al. (2021), the Permian metamorphic rocks were exposed in areas northwest of Lake Singkarak or south of Marapi Volcano. The Tertiary-aged rock units were exposed mainly to the east of GSF in the form of Eocene-Oligocene andesite basaltic rocks (Ts) and Mid-Miocene granite (Tmgr). The Quaternary-aged rocks are present in the forms of alluvium (Qal), hornblende hypersthene pumiceous tuff (Qhpt) produced by the eruption of Singgalang-Tandikat, Maninjau tuff (Qpt) produced by the eruption of Maninjau Caldera, and different andesites produced by the respective volcanoes, i.e., andesites of Marapi (Qama), andesites of Singgalang-Tandikat (Qast), and andesites of Maninjau Caldera (Qamj). A combination of fission-track and 14C dating reveals that the age of Maninjau pyroclastic deposits is 52 ± 3 ka (Alloway et al., 2004).

Data and methods

A ground geomagnetic survey was carried out in the following districts/municipalities in the West Sumatran Province: Agam, Padang Pariaman, Bukittinggi, and Padang Panjang using the GEM Proton Precision Magnetometers type GSM-19T (GEM System, Markham, Canada). Survey points (507 in total) were measured along the roads accessible to motorized vehicles. To minimize magnetic noise, the actual measurements were carried out up to 200 m from the roads, avoiding traffic, power lines, houses, and parked vehicles. The previous magnetic data (shown as red survey points in Figure 1B) from Amir et al. (2021) were integrated seamlessly with the new data from the 2021 survey (shown as blue survey points in Figure 1B). Because all the data was collected by the same people using the same instruments, it was combined without any correction. As shown in Figure 1B, the survey area is mountainous, preventing access to high elevation areas so that survey points are not uniformly distributed, affecting the quality of magnetic data.

The distance between two survey points varies between 500 and 1000 m. A Garmin GPS system was used to determine the coordinates of each survey point. The raw magnetic data was then corrected by diurnal and by IGRF (International Geomagnetic Reference Field) corrections to obtain the final magnetic intensity values. Figure 1B shows the distribution of survey points in the topographic map, combining the 507 new data points with 72 data points from Amir et al. (2021). Figure 2A shows the magnetic intensity anomaly map of the studied area. The magnetic data is displayed in the UTM coordinate system (metric system) for the 47 S zone to facilitate quantitative interpretation. Like that of Amir et al. (2021), this study also digitized all the contour lines in the Bouguer anomaly maps of Solok and Padang (Buyung et al., 1992a; 1992b) to obtain

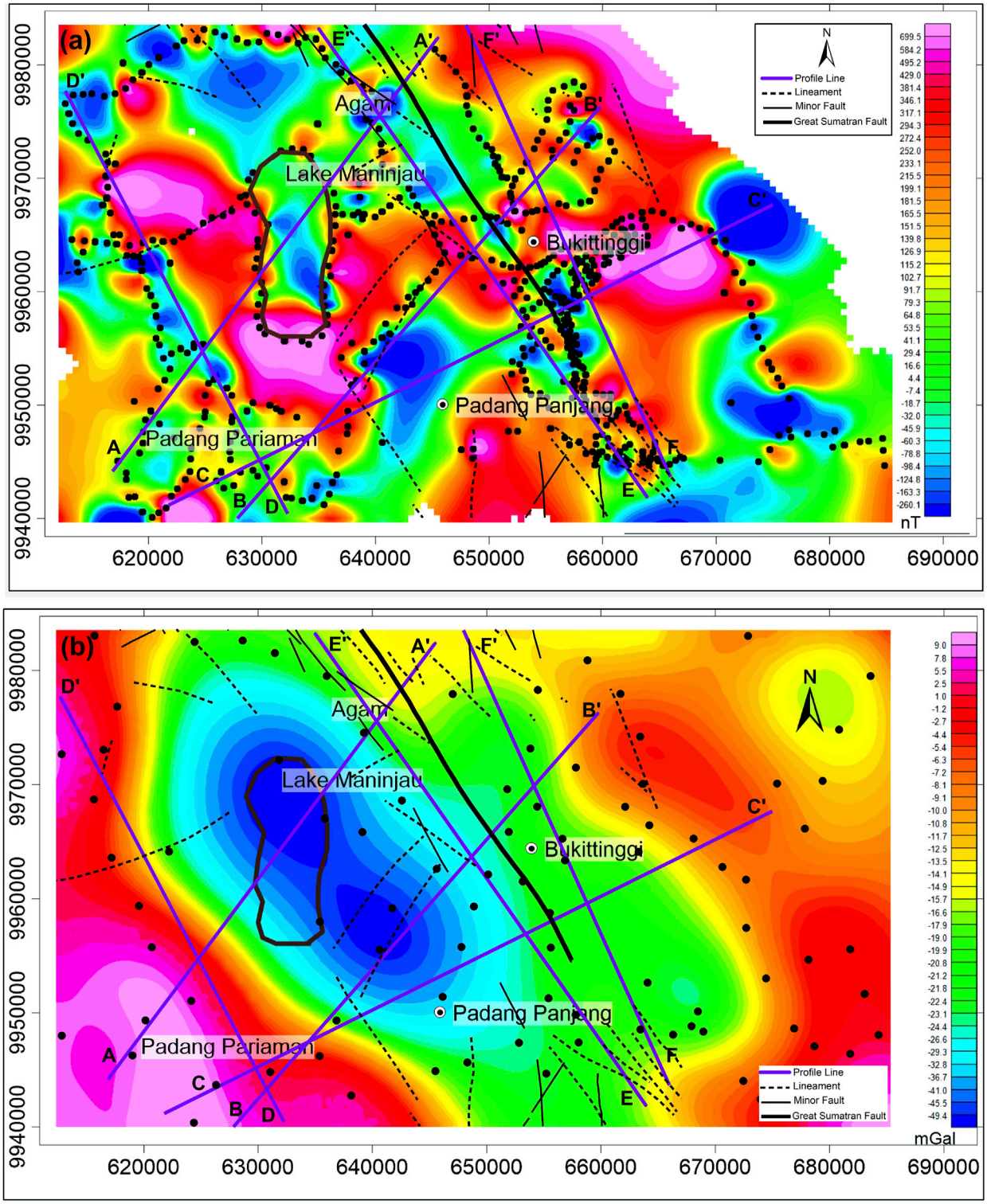

FIGURE 2
(A) The filtered magnetic anomaly map of the Sianok segment along with the six profiles discussed in this study. **(B)** A gravity anomaly map of the Sianok segment obtained by digitizing Buyung et al. (1992a; 1992b) Bouguer anomaly maps in the same area as **(A)**. Black circles are magnetic and gravity survey points.

the Bouguer anomaly map of the study area. The gravity contours were digitized as the only available information is in the form of the Bouguer Anomaly maps. As the surveys were conducted more than 30 years ago, the respective digital data is no longer available. Based on the information from the above maps, the correction density for the Bouguer anomaly is 2.67 gr/cc. Figure 2B shows the digitized Bouguer anomaly map of the study area along with the positions of gravity survey points displayed in the UTM coordinate system for the 47 S.

The Oasis Montaj GM-SYS version 6.4.2 (Geosoft Inc, Toronto, Canada) was used to incorporate gravity data and magnetic data so that they could be processed further. Based on the magnetic anomaly map shown in Figure 2A as well as on the distribution of measured and observed data, six profile lines (A-A′, B-B′, C-C′, D-D′, E-E′, and F-F′) were selected for modeling and analysis. The profiles of A-A′, B-B′, and C-C′ were selected as they cross interesting surface features on the gravity and magnetic maps. The profiles of D-D′, E-E′, and F-F′ were selected to identify the slivers of Permian metamorphic rock and unexposed intrusion (if any) that have been reported earlier by Amir et al. (2021). Such bodies are responsible for magnetic anomalies in the adjacent Sumani segment (Amir et al., 2021). Moreover, profiles E-E′ and F-F′ pass through outcrops of Permian metamorphic rocks, mainly in the southeast corner of the survey area. Despite it passing through a rather homogeneous rock outcrop, profile D-D' was chosen as it passes through several magnetic anomalies.

Interactive 2D magnetic and gravity models were calculated. As survey points were not distributed evenly in the grid system, Oasis Montaj extrapolates and interpolates data at any point 250–1000 m from the survey points so that the overall anomaly maps represent grid points. As magnetic survey points are denser than gravity survey points, the grid cell size of magnetic data is 250 m while that of gravity data is 500 m. The blanking distance parameter was set at a value of 5000 m, which was used in the extrapolation technique for the distribution of measurement points.

Interactive forward modeling processes were carried out on both magnetic and gravity data using Oasis Montaj to obtain a suitable subsurface geological model represented by a series of polygons. The shape of each polygon was controlled by its geological structure. Each polygon was given its own values of magnetic susceptibility and density based on the type of rock. For each of the six profile lines, the best model of its subsurface structure is determined by the good match between the observed and calculated data. Using methods described in Amir et al. (2021), a total of 24 rock samples were measured for their magnetic susceptibilities and densities. However, instead of the MS2 magnetic susceptibility meter, the newer MS3 meter was used with the MS2B sensor (Bartington Instruments Ltd., Oxford, UK). The results of such measurements are listed in Table 1. Results by Amir et al. (2021) from the nearby Sumani Segment of GSF were also used to initiate the modelling processes, especially for the basement rocks. Due to their proximity, the basement rocks of the Sianok Segment are similar to those of the Sumani Segment. However, as pointed out by Barber and Crowe (2005) and by Setiawan et al. (2017), basement rocks are not homogeneous nor well-defined. Therefore, to obtain a good fit for the observed anomalies, lateral variations are acceptable. Potential methods in geophysics (such as gravity and magnetic methods), intrinsically, contain non-uniqueness. Therefore, despite all the efforts to obtain dependable models, the models generated in this study are not unique.

Results

Results of magnetic susceptibility and density measurements are presented in Table 1. Although the three andesitic groups (Marapi, Singgalang-Tandikat, and Maninjau) have similar average densities, their magnetic susceptibilities vary significantly, with Singgalang-Tandikat samples having the highest average susceptibility. Such variations might be due to variations in Fe content in these igneous rocks. As expected, due to its high silicate content, the Maninjau tuff (Qpt) has low average density of only 2.10 g/cm^3 and has a low magnetic susceptibility. The Permian metamorphic rock samples have a

TABLE 1 Magnetic susceptibility and density values of outcrop samples around the Sumani segment. *N* is number of measured samples while STD is the standard deviation. See Figure 1 for lithological terms.

Type/Lithology	N	Susceptibility × 10^{-5} cgs-unit			Density (g/cm^3)		
		Range	Average	STD	Range	Average	STD
Igneous (Andesite of Marapi, Qama)	6	67.35–109.64	87.32	16.54	2.45–2.63	2.56	0.06
Igneous (Andesite of Maninjau, Qamj)	6	1.06–79.71	38.32	36.88	2.55–2.74	2.60	0.06
Igneous (Andesite of Singgalang-Tandikat, Qast)	6	116.30–151.96	130.89	14.46	2.56–2.62	2.59	0.02
Metamorphic (Permian metamorphic, Ps)	3	0.10–0.18	0.15	0.03	2.44–2.55	2.49	0.05
Volcanic Deposit (Maninjau tuff, Qpt)	3	0.16–0.17	0.16	0.01	1.91–2.35	2.10	0.18

N is number of measured samples while STD, is the standard deviation.

sizable density averaging 2.49 g/cm^3 and much lower magnetic susceptibility compared to igneous rocks.

Profile A-A′

Figure 3 shows the results of magnetic and gravity modeling which intersects the middle of Lake Maninjau and the GSF trending NW-SE. This 48 km section shows the subsurface structures in the 20 km image and the more detailed 10 km image. The magnetic anomalies are mainly due to the shallow magma chamber beneath the Maninjau Caldera, the andesites of Maninjau Caldera (Qamj), and the sliver of Permian metamorphic rocks. The presence of gravity low in the middle of the profile is associated with the Maninjau Caldera collapse, whose density is lower than that of basement rocks. The models in Figure 3 show that the Maninjau tuff deposits (Qpt) as well as the andesites of Maninjau Caldera (Qamj) are 1 and 3.5 km thick. The models also show Permian metamorphic rocks (Ps) in some locations could be as thick as 3.9 km (in vertical dimension).

Profile B-B′

The profile B-B' (Figure 4) is located between the Maninjau Caldera and Mount Singgalang-Tandikat and shows the GSF and Maninjau tuff in the northeast. As shown in Figure 4, the magnetic anomalies in this profile are interpreted as due to the Maninjau tuff (Qpt), hornblende hypersthene pumiceous tuff (Qhpt), andesites of Singgalang-Tandikat (Qast), and exposed as well as unexposed Permian metamorphic rocks. The shallow magma chamber of Singgalang-Tandikat might also contribute to these magnetic anomalies. The unexposed metamorphic rocks are located under Quaternary volcanic deposits. The high gravity in the southwest is associated with lower basement rocks, while the low gravity in the middle is associated with Maninjau Caldera collapsed with lower density. At shallower depths, the metamorphic rocks were exposed on the SE side of profile B-B' and extended further to a depth of up to 4 km. On the surface, further NE along profile B-B′, there are deposits of carboniferous carbonate rocks (Cl) on top of the metamorphic rocks.

Profile C-C′

As shown in Figure 5, the 60 km long profile C-C′ starts in the southwest in the same area as the B-B′ profile. In the SW-NE direction, the profile intersects the middle of Mount Singgalang-Tandikat, GSF, and the north part of Mount Marapi. Based on modeling in this study, the magnetic anomalies are associated with two shallow magma bodies (see Figures 1A, 2A), the andesites of Marapi (Qama), the andesites of Singgalang-Tandikat (Qast), and slivers of Permian metamorphic rocks. The two shallow magma bodies are interpreted, subsequently, as the shallow magma chambers of Marapi and Singgalang-Tandikat. The SW part of profile C-C' is marked by high gravity associated with lower basement rocks and the middle low gravity associated with low density Maninjau Caldera Structure, while the NE part of this profile is marked by high gravity associated with denser basement rocks and thick layers of Permian metamorphic rocks. There are subsequent layers of basement, metamorphic rocks, and andesite volcanic rocks of Mount Singgalang-Tandikat and Mount Marapi deposited at the surface. The geological structure below the area between Mount Singgalang-Tandikat and Mount Marapi could be more complicated where the Sianok Segment and Sumani Segment end.

Profile D-D′

As shown in Figure 6, the 42 km long D-D′ profile is on the western side of Lake Maninjau in a SE-NW direction. Based on modeling in this study, the magnetic anomalies are associated with the presence of Permian metamorphic layers along the profile (see Figures 1A, 2A) as well as the andesites of Maninjau (Qamj). The gravity anomaly is higher in the SE part compared to the middle and high gravity in the NW part. The low gravity in the middle part is likely to be attributed to the relatively low density of the Maninjau Caldera Collapse. It is likely that Maninjau tuff in the SE and in the NW of the Profile D-D' shows significant thickness.

Profile E-E′

The 60 km long E-E′ profile is located along the west side of GSF, parallel to profile F-F' (see Figures 1A, 2A). Figure 7 shows the great variation of magnetic anomalies, representing the great variation of surface rocks. The anomalies are due to andesites of Marapi (Qama), andesites of Singgalang-Tandikat (Qast), exposed Permian metamorphic rocks, and Maninjau tuff (Qpt). These magnetic anomalies might also be attributed to the shallow magma chamber of Singgalang-Tandikat. Figure 7 shows a negative gravity anomaly at the middle of the profile. This might have been caused by relatively less dense basement rocks (close to Maninjau Caldera) and at the surface related to Andesite of Singgalang-Tandikat and Andesite of Maninjau, and the lower density of Maninjau tuff compared to that underneath the SE and NW end of the profile E-E′.

Profile F-F′

The profile F-F′ is located along the east side of GSF parallel to profile E-E′ (see Figure 2). As shown in Figure 8, the 44 km

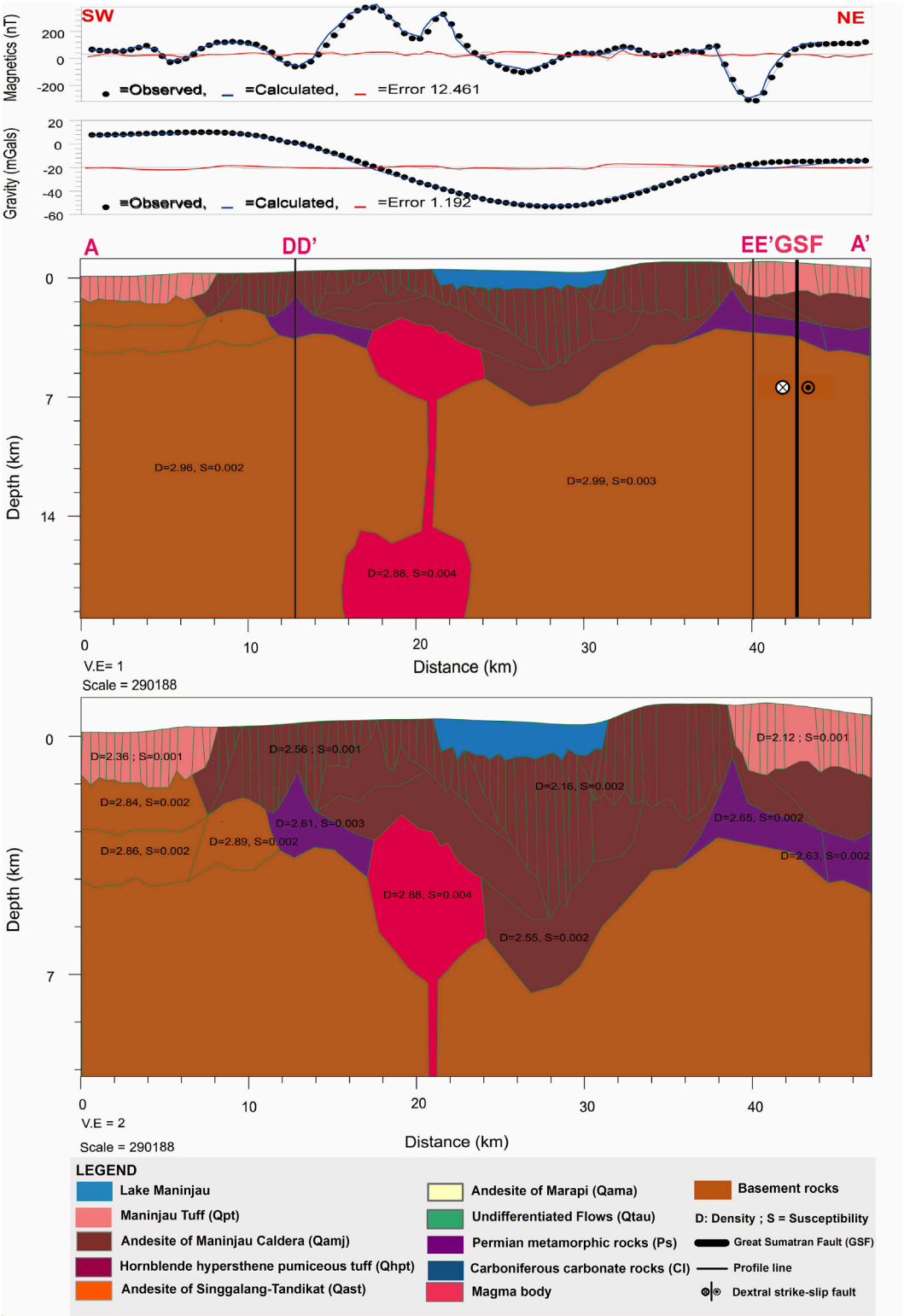

FIGURE 3
2D modeling of magnetic and gravity data of the A-A′ profile in the Sianok segment of GSF showing the subsurface structures beneath Maninjau Caldera that include shallow and deep magma chambers. Models are presented in a more general 20 km deep image and a more detailed 10 km deep image.

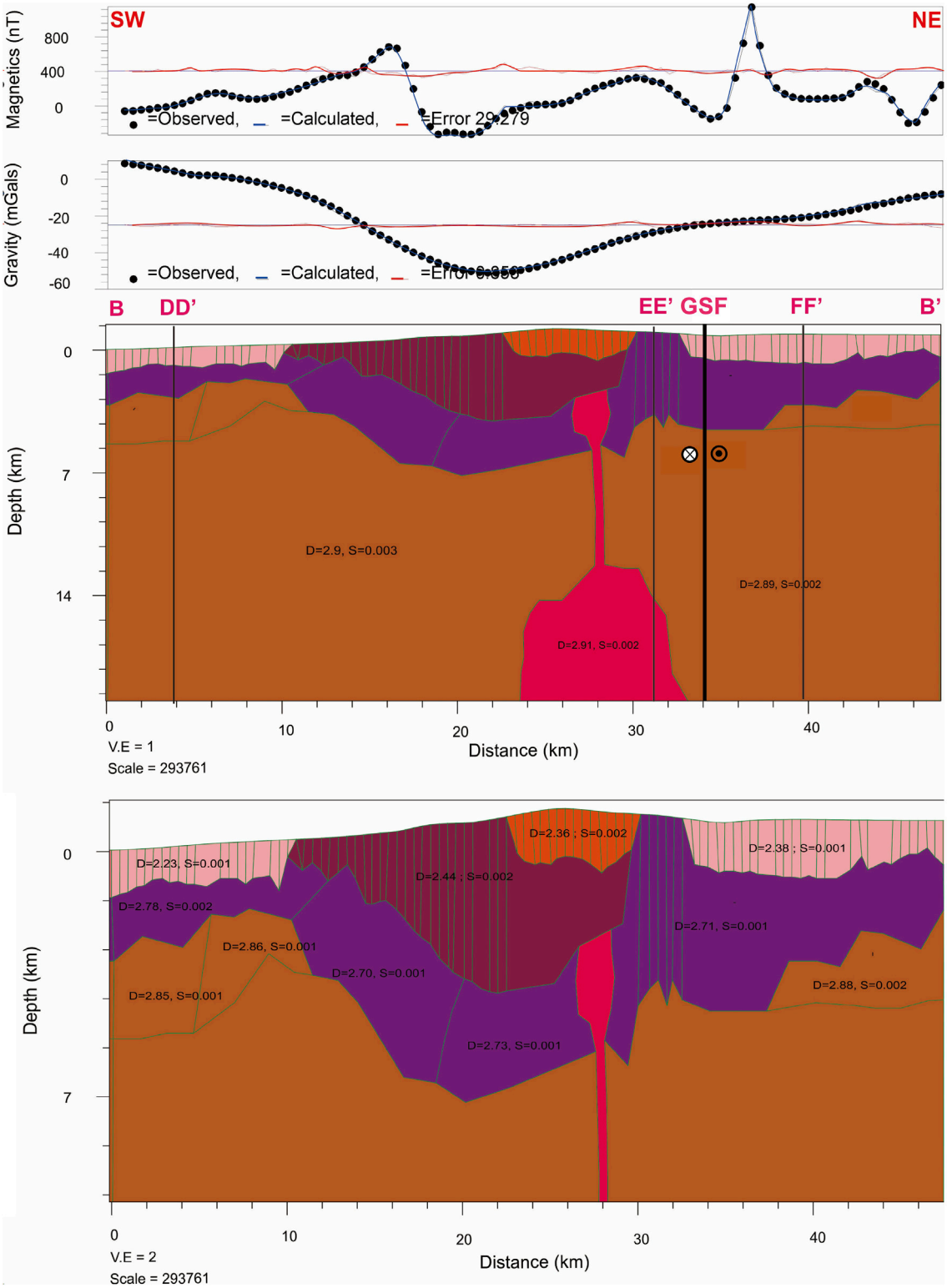

FIGURE 4
2D modeling of magnetic and gravity data of the B-B′ profile in the Sianok segment of GSF shows the subsurface structures beneath Mount Singgalang-Tandikat that include its shallow and deep magma chambers. This model also shows slivers of Permian metamorphic rocks encased in the basement rocks. This figure uses the same legend as that in Figure 3.

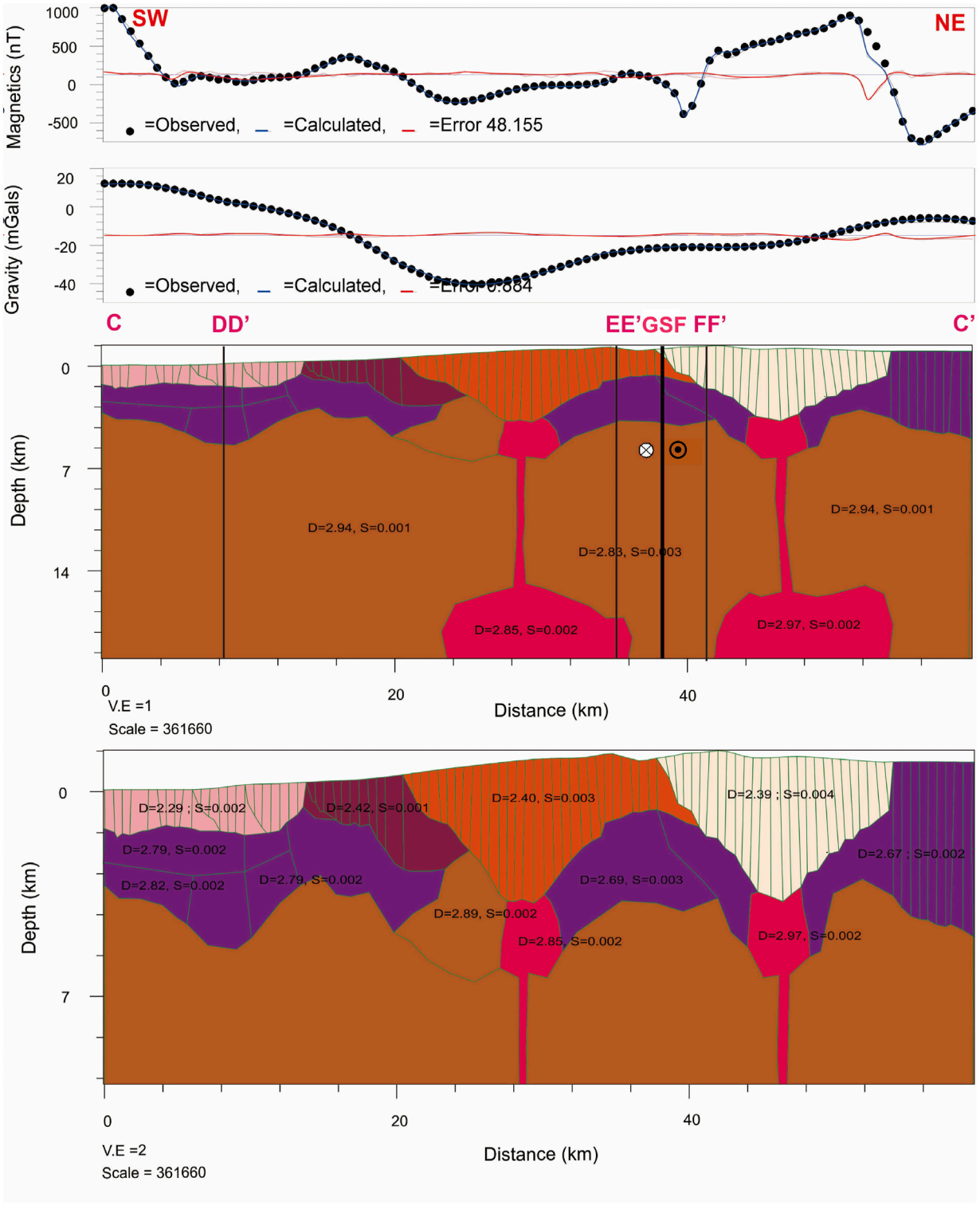

FIGURE 5
2D modeling of magnetic and gravity data of the C-C′ profile in the Sianok segment of GSF showing the subsurface structures beneath Mount Singgalang-Tandikat and beneath Mount Marapi that include their shallow and deep magma chambers. Note that the deep magma chamber of Marapi is significantly shallower than that of Singgalang-Tandikat. This figure uses the same legend as that in Figure 3.

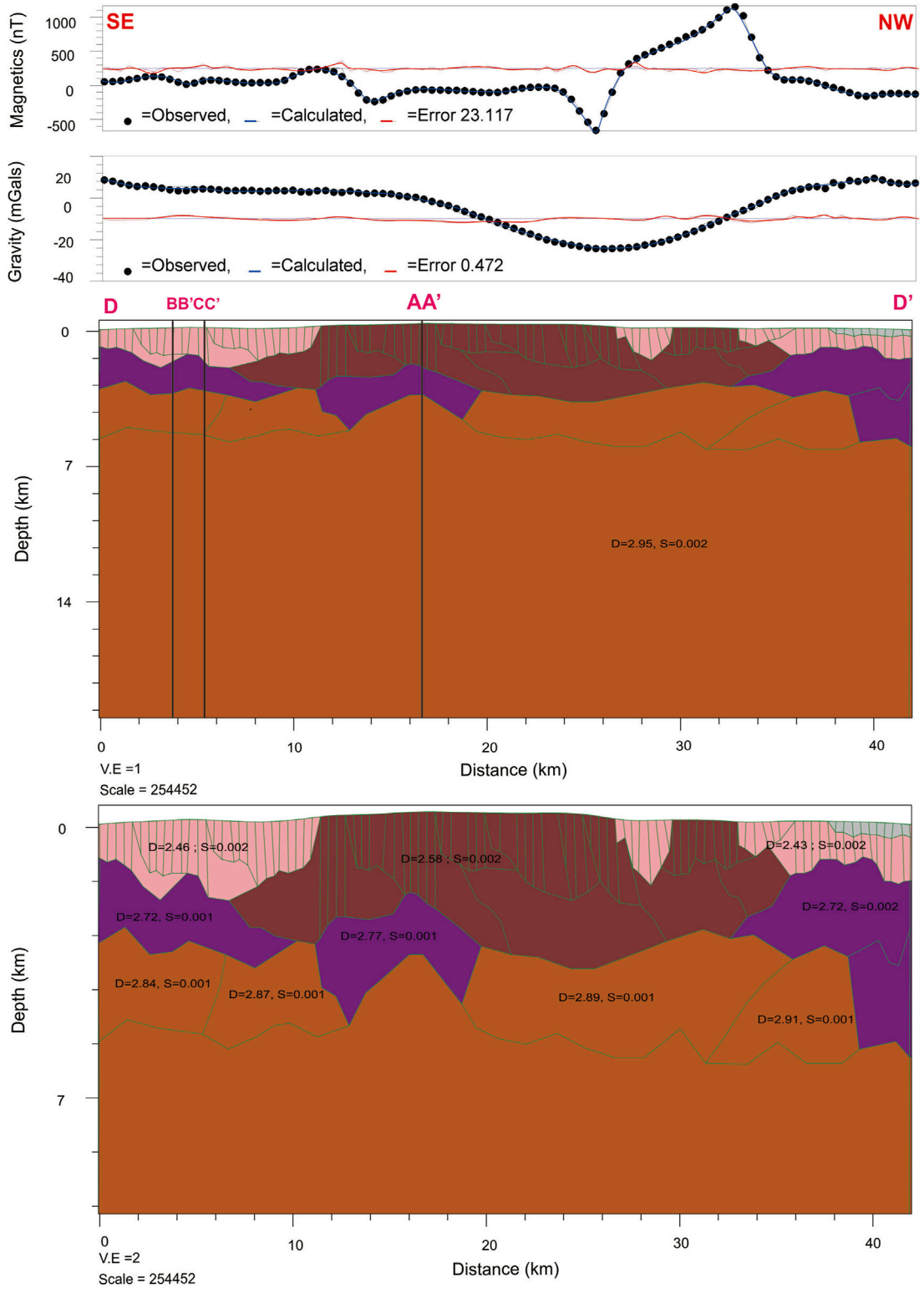

FIGURE 6
2D modeling of magnetic and gravity data of the D-D′ profile in the Sianok segment of GSF showing slivers of Permian metamorphic rocks encased in the basement rocks. See the text for details. This figure uses the same legend as that in Figure 3.

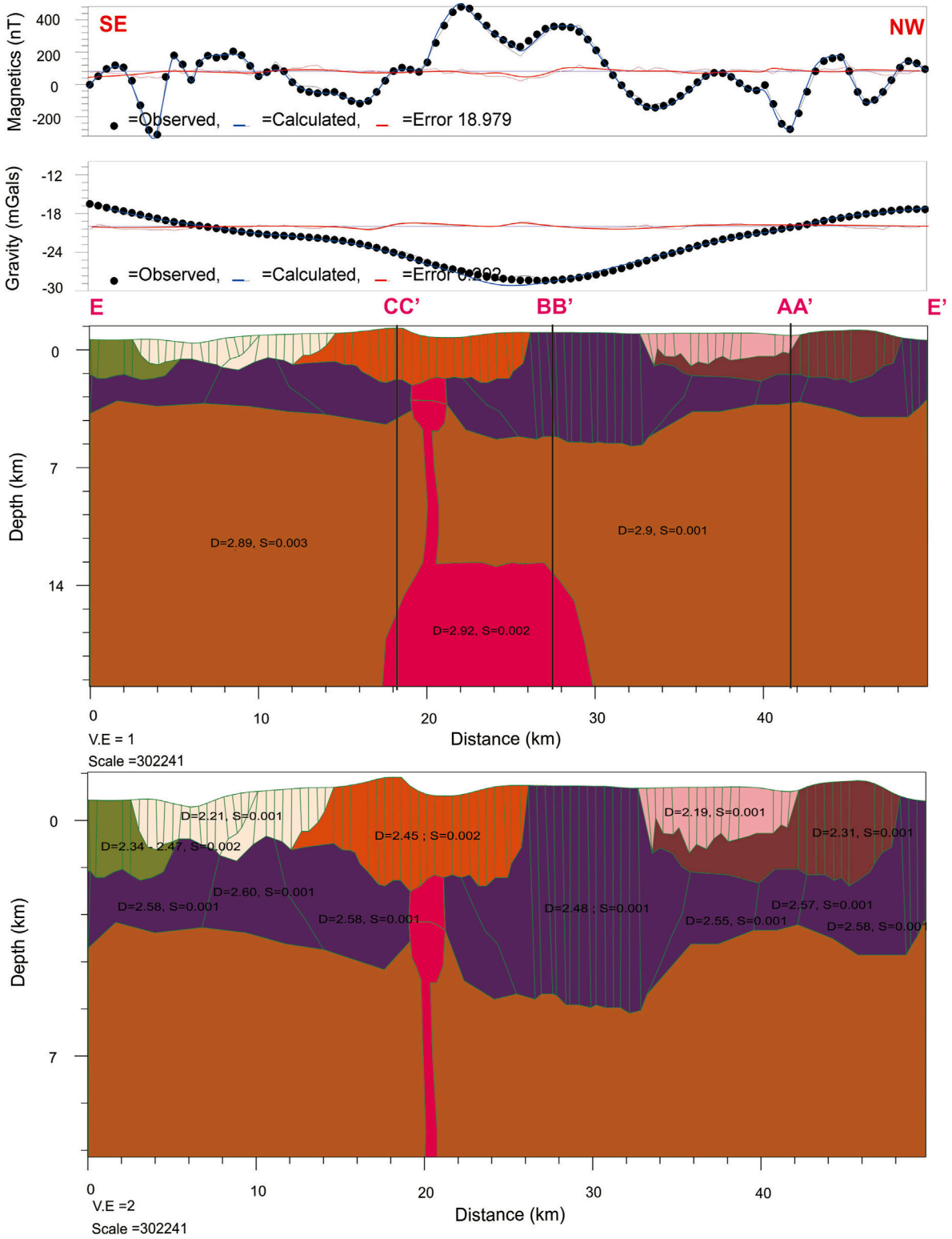

FIGURE 7
2D modeling of magnetic and gravity data of the E-E′ profile in the Sianok segment of GSF showing the shallow and deep magma chambers of Mount Singgalang Tandikat. This segment passes different surface lithologies (Qamj, Qpt, Ps, Qast, and Qama), causing variation in the measured surface magnetic anomalies. As presented in Table 1, these surface lithologies vary in their average magnetic susceptibilities. See the text for details. This figure uses the same legend as that in Figure 3.

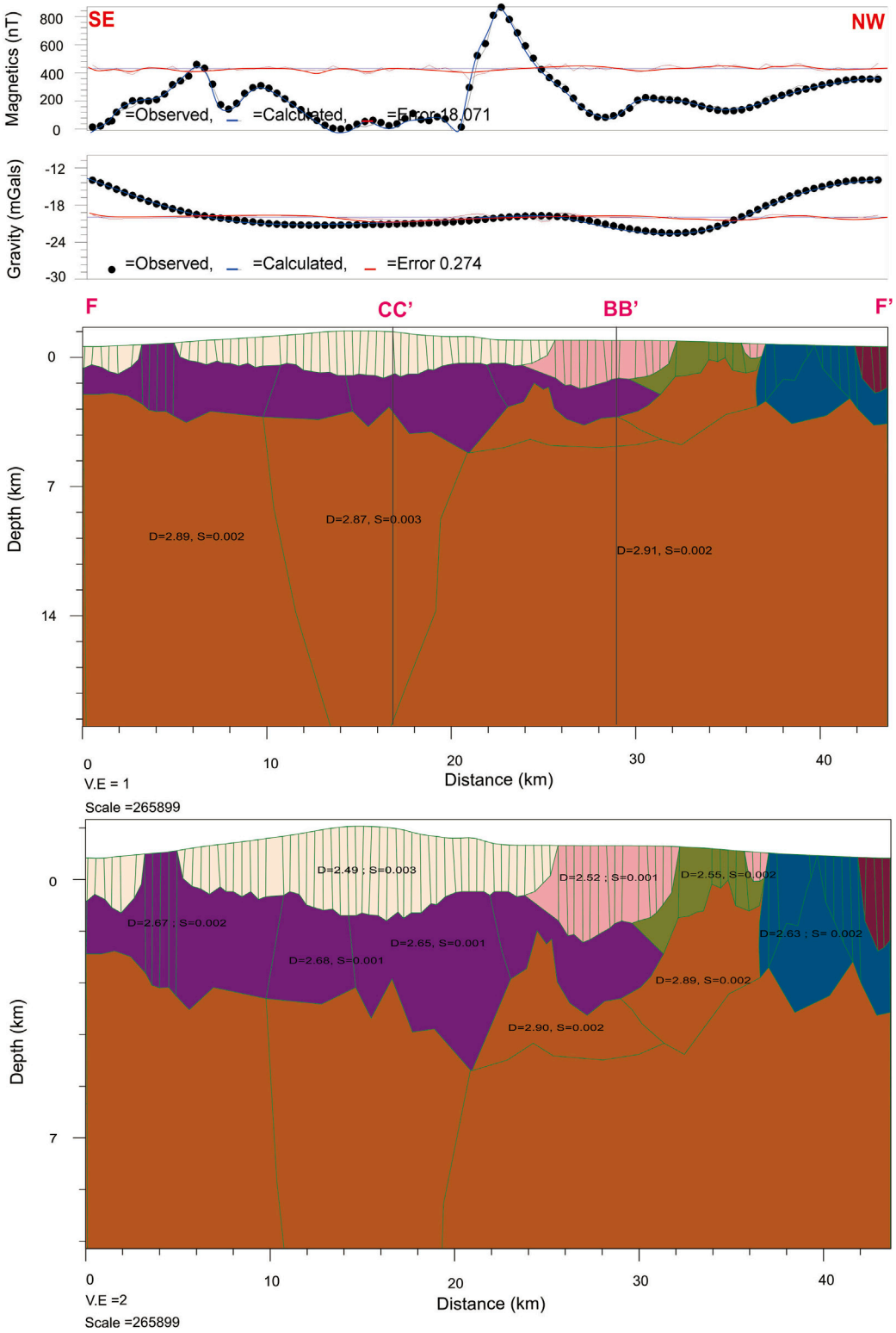

FIGURE 8
2D modeling of magnetic and gravity data of the F-F′ profile in the Sianok segment of GSF. See the text for details. This figure uses the same legend as that in Figure 3.

long profile shows that the magnetic anomalies in this profile are mainly attributed to the andesites of Marapi (Qama), Maninjau tuff (Qpt), exposed and unexposed Permian metamorphic rocks, and Carboniferous carbonate rocks (Cl). As shown in Figure 2B, this profile passes through an area with a small variation in gravity anomalies.

Discussion

Based on 2D models of magnetic and gravity data, this study identifies two magma chambers beneath Mount Merapi and Singgalang-Tandikat as well as beneath the Maninjau Caldera. As shown in Figure 3, the relatively small and shallow magma chamber beneath Maninjau Caldera is located at a depth of about 6 km. This agrees with the proposed depth given by Suhendro (2021), who argued that the pumice of the 52 ka eruption was produced partly by a reservoir at a depth of ≤5.8 km (stable condition for quartz crystallization) and partly by a reservoir at ≥5.8 km (stability limit of hornblende). Figure 5 shows the shallow magma chambers of Mount Marapi and Mount Singgalang-Tandikat are located at a depth of about 5 km. The depth of the shallow magma chamber beneath Mount Marapi agrees with the models of Nurfiani et al. (2021) derived from geothermobarometry and seismic receiver function methods. The shape or geometry of these shallow magma chambers, however, is arbitrary and is not yet constrained by other methods. Both Figures 3, 5 also show the presence of deep magma chambers beneath the Maninjau Caldera as well as beneath Mount Marapi and Mount Singgalang-Tandikat. These deep magma chambers are modelled without sufficient constraint by gravity and magnetic data. Therefore, the depths and shapes of these magma chambers should not be trusted completely. The limitations in estimating deep magma chambers are not due to the models nor the data. Limitation originates from the physical nature of gravity and magnetic fields. The physics of magnetic and gravity fields dictate that deep bodies, such as the deep magma chambers, have lower amplitudes of magnetic and gravity anomalies. These deep bodies would also have broader anomalies. In any case, the deep magma chambers of Maninjau Caldera, Mount Marapi, and Mount Singgalang-Tandikat are significantly shallower than the depth of the deep magma chamber beneath Toba Caldera (30–50 km deep) (Koulakov et al., 2016).

According to Purbo-Hadiwidjoyo et al. (1979), Maninjau's eruption produced broad and thick tuff deposits that are 220–250 km^3 in volume. Suhendro (2021) argued that Maninjau's 52 ka eruption is of similar type to that of Toba's eruption and Ranau's eruption but differs from the eruptions of Krakatau, Samalas, and Tambora. In Maninjau's 52 ka eruptions, there is no Plinian ash-fall deposit between paleosoil and ignimbrite deposits (Suhendro, 2021). Early theoretical work by Wilson et al. (1980) suggested that the types of eruption depend not only on magma types and their volumes but also on the size of conduits. The presence and activities of GSF near Maninjau, Toba, and Ranau might affect the size of their conduits. Larger conduits allow high decompression rates, causing the release of large volumes of material in a brief time.

How could GSF affect the size of magma conduits beneath Maninjau? When magma rises through the Earth's crust, there is a change in the physical properties of the surrounding crust with increasing temperature, and part of the crust can change from solid to liquid (Gill, 2010). Earlier, Costa and Marti (2016) showed that the sustainable dimension of a dyke conduit beneath a volcano depends on the extensional far-field stress. This implies that the area around the intrusion will be more easily deformed. Due to the strike-slip stress distribution along the GSF zone, the area around a large magma intrusion tends to form an extensional stress similar to that of pull-apart stress. Therefore, stress extension in the intrusion area might enlarge the conduit from the deep magma pocket to the surface.

Figure 2B shows a large negative gravity anomaly beneath Maninjau Caldera caused by the eruption products that collapse inside the caldera, replacing materials released during the eruption. Figure 3 shows a sizable deposit (of up to 5–6 km deep) of Maninjau's andesite and other eruption products. The measurement of density in this study shows that the Maninjau tuff samples have an average density as low as 2.10 gr/cm^3 (see Table 1). Such a negative gravity anomaly is also observed beneath Toba's caldera (Nishimura et al., 1984). In contrast, Figure 2A shows large positive and negative magnetic anomalies in the vicinity of the Maninjau Caldera, especially in its W and SW areas. These anomalies, according to Figure 3, relate to the subsurface structures located on the west side of the caldera. Apart from Maninjau's andesite itself, the other structure that might be responsible for these anomalies is the shallow magma chamber. This situation is similar to that in Toba's caldera, where the position of the magma chamber is located beneath the west side of the caldera (Stankiewicz et al., 2010; Koulakov et al., 2016). It will be interesting to study whether the magma chamber of the youngest caldera in the GSF, i.e., Ranau's caldera, erupted in the late quaternary (Natawidjaja et al., 2017), is also located beneath the western part of the caldera. If so, then there is a pattern that the magma chambers of all major calderas in the vicinity of GSF are all located not beneath the calderas but rather beneath the western parts of calderas. Such a pattern might be crucial in understanding the interplay between fault development and volcanism in Sumatra.

This study also reveals the presence of encased Permian metamorphic rocks in the basement rock, as reported earlier by Amir et al. (2021) in the Sumani segment. The models infer that these bodies are common in the GSF and explain some localized

magnetic anomalies. If properly mapped on a regional scale, the distribution of encased Permian metamorphic rocks would be invaluable to the tectonic understanding of the GSF. These Permian metamorphic rocks were remnants of the Sundaland Continental Margin prior to the Mid-Cretaceous subduction (Barber, 2000).

The rate of change in tectonic stress along the GSF is certainly related to the rate of change in stress on the Sumatra subduction megathrust trough, which continues in arc-parallel sliver movement or stress change in the sliver plates and then changes the tectonic stress or strike-slip movement along the GSF. There are three factors that might affect the rate of change in tectonic stress along the GSF. The first one is changes in stress on the arc-parallel to sliver plate. The second one is the variation of rock rigidity in the GSF, and the third one is the geometry of geological structures in the GSF. The geology of the Sianok segment is affected significantly by two kinds of processes, namely tectonic and volcanic processes. Currently, Mount Marapi and Mount Singgalang Tandikat show high volcanic activity. The area between these two volcanoes, where the Sianok and Sumani segments meet (Sieh and Natawidjaja, 2000), was affected by a major earthquake in 1926 and a doublet earthquake in 2006 (Daryono et al., 2016).

Can this study identify the subsurface structure beneath the end of the Sianok segment? The extensive coverage of volcanic deposits on Mount Marapi and Mount Singgalang-Tandikat impedes the surface representation of GSF at the end of the Sianok segment. This coverage of volcanic deposits also makes accurate subsurface modelling difficult. Surface outcrops, which are not available in this study area, are often used to facilitate subsurface modelling. However, the magnetic anomalies in the range of—70 nT to 130 nT in the SE part of the studied area infer the high heterogeneity of subsurface structures. Therefore, such magnetic anomalies could be considered as indicators for the end of the Sianok segment.

This study serves as the first investigation of subsurface structures in the volcanic centers of the Central Barisan Fault identified by Posavec et al. (1973). The Marapi volcanic center of this study is in the vicinity of the boundary between the Sianok and Sumani segments. With the established segmentations of GSF (see Sieh and Natawidjaja, 2000), the other volcanic centers could also be identified as boundaries between GSF segments. Talang's volcanic center is situated between the Sumani and Suliti segments; Kerintji is situated between the Suliti and Siulak segments; Hulumajang is situated between the Siulak and Dikit segments; Pandan is situated between the Dikit and Ketaun segments; Kaba is situated between the Ketaun and Musi segments; and Dempo is situated between the Musi and Manna segments. This realization is interesting as well as important as studies similar to this study might be carried out in the future and provide fresh information on the interplay between fault development and volcanism in the GSF.

Conclusion

Analyses of magnetic and gravity data in this study have successfully identified the shallow magma chambers beneath the Maninjau Caldera as well as beneath Mount Marapi and Mount Singgalang-Tandikat. The magnetic anomalies in the Sianok segment are mainly due to thick deposits of Maninjau Caldera's andesites as well as andesites of Marapi and Singgalang-Tandikat. Slivers of Permian metamorphic rocks encased in the basement rock also contribute to these anomalies. The noticeable negative gravity anomalies in Maninjau Caldera are likely associated with the Maninjau Caldera collapse, where lighter rocks produced during eruption were accumulated in the caldera. The models also show that the Maninjau tuff deposits are also quite thick, with a thickness of about 1 km. This study also reveals that exposed and unexposed Permian metamorphic rocks are common in the Sianok segment, similar to those reported earlier in the Sumani segment. The models corroborate the depth of shallow magma chambers beneath Mount Marapi (5 km) and beneath Maninjau Caldera (6 km), estimated by previous estimation using petrographic analyses, geothermobarometry, and seismic receiver function. Our models also show that the depth and size of the shallow magma chamber beneath Mount Singgalang-Tandikat is roughly similar to that of Mount Marapi. Although this study also modelled deep magma chambers beneath Maninjau Caldera, Mount Marapi, and Mount Singgalang-Tandikat, the depth and geometry of these deep magma chambers cannot be fully constrained Pribadi et al., 2007.

Data availability statement

The raw data supporting the conclusions of this article will be made available by the authors, without undue reservation.

Author contributions

DD, HA, and SB conceived the study. All authors, except for IA and KI, participated in the field survey. DD, HA, PS, SB, SF, and IA processed, analyzed, and interpreted the data. DD, HA, PS, and SB collected the rock samples while KI measured their density and the magnetic susceptibilities. KI also prepared the maps and figures in this study. DD, HA, PS, SB, SF, and UH contributed to the preparation of the manuscript. All authors read and approved the final manuscript.

Funding

This study was made possible by funding from the Ministry of Education, Culture, Research, and Technology of the Republic

of Indonesia through contract #2/AMD/E1/KP.PTNBH/2020 to DD (PDUPT grant) and #2/E1/KP.PTNBH/2021 to SB (PDD grant). Article processing fee for this publication was made possible by the 2022 PPMI grant from Institut Teknologi Bandung to Applied and Exploration Geophysics Research Group. The 2022 PPMI grant was administered by the Faculty of Mining and Petroleum Engineering of Institut Teknologi Bandung.

Acknowledgments

The authors thank the Ministry of Education, Culture, Research and Technology of the Republic of Indonesia for its financial support through contract # 2/AMD/E1/KP.PTNBH/2020 to DD (PDUPT grant) and # 2/E1/KP.PTNBH/2021 to SB (PDD grant). The Provincial Government of West Sumatra is thanked for its permission to conduct this study. HA received a doctoral scholarship from Padang State University. The two reviewers are thanked for their constructive comments and criticism that helped the authors improve the quality and clarity of this manuscript.

Conflict of interest

The authors declare that the research was conducted in the absence of any commercial or financial relationships that could be construed as a potential conflict of interest.

Publisher's note

All claims expressed in this article are solely those of the authors and do not necessarily represent those of their affiliated organizations, or those of the publisher, the editors and the reviewers. Any product that may be evaluated in this article, or claim that may be made by its manufacturer, is not guaranteed or endorsed by the publisher.

References

Acocella, V., Bellier, O., Sandri, L., Sébrier, M., and Pramumijoyo, S. (2018). Weak tectono-magmatic relationships along an obliquely convergent plate boundary: Sumatra, Indonesia. *Front. Earth Sci.* 6, 3. doi:10.3389/feart.2018.00003

Acocella, V. (2014). Structural control on magmatism along divergent and convergent plate boundaries: Overview, model, problems. *Earth. Sci. Rev.* 136, 226–288. doi:10.1016/j.earscirev.2014.05.006

Alloway, B. V., Pribadi, A., Westgate, J. A., Bird, M., Fifield, L. K., Hogg, A., et al. (2004). Correspondence between glass-FT and ^{14}C ages of silicic pyroclastic flow deposits sourced from Maninjau Caldera, west-central Sumatra. *Earth Planet. Sci. Lett.* 227, 121–133. doi:10.1016/j.epsl.2004.08.014

Amir, H., Bijaksana, S., Dahrin, D., Nugraha, A. D., Arisbaya, I., Pratama, A., et al. (2021). Subsurface structure of Sumani segment in the Great Sumatran Fault inferred from magnetic and gravity modeling. *Tectonophysics* 821, 229149. doi:10.1016/j.tecto.2021.229149

Ammon, C. J., Ji, C., Thio, H. K., Robinson, D., Ni, S., Hjorleifsdottir, V., et al. (2005). Rupture process of the 2004 sumatra-andaman earthquake. *Science* 308, 1133–1139. doi:10.1126/science.1112260

Araffa, S. A., El-bohoty, M., Abou Heleika, M., Mekkawi, M., Ismail, E., Khalil, A., et al. (2018). Implementation of magnetic and gravity methods to delineate the subsurface structural features of the basement complex in central Sinai area, Egypt. *NRIAG J. Astronomy Geophys.* 7, 162–174. doi:10.1016/j.nrjag.2017.12.002

Barber, A. J., and Crow, M. J. (2005). "Pre-Tertiary stratigraphy,".*Sumatra Geol. Resour. Tect. Evol.* Editors A. J. Barber, M. J. Crow, and J. S. Milsom (Geol. Soc., London Mem), 31, 24–53.

Barber, A. J. (2000). The origin of the woyla terranes in Sumatra and the late mesozoic evolution of the Sundaland margin. *J. Asian Earth Sci.* 18, 713–738. doi:10.1016/S1367-9120(00)00024-9

Bellier, O., and Sebrier, M. (1995). Is the slip rate variation on the Great Sumatran Fault accommodated by fore-arc stretching? *Geophys. Res. Lett.* 22, 1969–1972. doi:10.1029/95GL01793

Bellier, O., Sébrier, M., Pramumijoyo, S., Beaudouin, T., Harjono, H., Bahar, I., et al. (1997). Paleoseismicity and seismic hazard along the great Sumatran Fault (Indonesia). *J. Geodyn.* 24, 169–183. doi:10.1016/S0264-3707(96)00051-8

Bradley, K. E., Feng, L., Hill, E. M., Natawidjaja, D. H., and Sieh, K. (2017). Implications of the diffuse deformation of the Indian Ocean lithosphere for slip partitioning of oblique plate convergence in Sumatra. *J. Geophys. Res. Solid Earth* 122, 572–591. doi:10.1002/2016JB013549

Burton, P. W., and Hall, T. R. (2014). Segmentation of the Sumatran Fault. *Geophys. Res. Lett.* 41, 4149–4158. doi:10.1002/2014GL060242

Buyung, N., Mirnanda, E., and Walker, A. S. D. (1992b). *Bouguer anomaly map of the Solok quadrangle, sumatera*. Bandung: Geological Research and Development Center.

Buyung, N., Subagioand Walker, A. S. D. (1992a). *Bouguer anomaly map of the Padang quadrangle, sumatera*. Bandung: Geological Research and Development Center.

Costa, A., and Martí, J. (2016). Stress field control during large caldera-forming eruptions. *Front. Earth Sci.* 4, 92. doi:10.3389/feart.2016.00092

Daryono, M. R., Natawidjaja, D. H., and Sieh, K. (2012). Twin-surface ruptures of the march 2007 M>6 earthquake doublet on the Sumatran Fault. *Bull. Seismol. Soc. Am.* 102, 2356–2367. doi:10.1785/0120110220

Daryono, M. R. (2016). *Paleoseismology of tropical Indonesia (case study is Sumatran Fault, Palukoro Fault and Lembang Fault)*. Bandung: Institut Teknologi Bandung (Dissertation).

Daryono, M. R., and Tohari, A. (2016). Surface rupture and geotechnical features of the July 2, 2013, Tanah Gayo earthquake. *Indones. J. Geosci.* 3, 95–105. doi:10.17014/ijog.3.2.95-105

Duquesnoy, T., Bellier, O., Kasser, M., Sebrier, M., Vigny, C., and Bahar, I. (1996). Deformation related to the 1994 Liwa earthquake derived from geodetic measurements. *Geophys. Res. Lett.* 23, 3055–3058. doi:10.1029/96GL02818

Genrich, J. F., Bock, Y., McCaffrey, R., Prawirodirdjo, L., Stevens, C. W., Puntodewo, S. S. O., et al. (2000). Distribution of slip at the northern Sumatran fault system. *J. Geophys. Res.* 105, 28327–28341. doi:10.1029/2000jb900158

Gill, R. (2010). *Igneous rocks and processes: A practical guide*. Oxford, UK: Wiley Blackwell.

Gunawan, E., Widiyantoro, S., Rosalia, S., Daryono, M. R., Meilano, I., Supendi, P., et al. (2018). Coseismic slip distribution of the 2 July 2013 Mw 6.1 Aceh, Indonesia, earthquake, and its tectonic implications. *Bull. Seismol. Soc. Am.* 108, 1918–1928. doi:10.1785/0120180035

Hamilton, W. (1979). *Geological Survey Professional Paper 1078*. Washington, DC, USA: US Govt Printing Office.Tectonic of the Indonesian region.

Hinze, W. J., Frese, R. R. B., and Saad, A. H. (2012). *Gravity and magnetic exploration: Principles, practices, and applications*. New York, NY, USA: Cambridge University Press.

Ito, T., Gunawan, E., Kimata, F., Tabei, T., Meilano, I., Ohta, Y., et al. (2016). Co-seismic offsets due to two earthquakes (Mw 6.1) along the Sumatran fault system derived from GNSS measurements. *Earth Planets Space* 68, 57. doi:10.1186/s40623-016-0427-z

Ito, T., Gunawan, E., Kimata, F., Tabei, T., Simons, M., Meilano, I., et al. (2012). Isolating along-strike variations in the depth extent of shallow creep and fault locking on the northern Great Sumatran Fault. *J. Geophys. Res.* 117, B06409. doi:10.1029/2011JB008940

Jiang, S., Gao, S., Li, S., Zhang, H., and Zhao, F. (2007). Gravity-magnetic anomaly and tectonic units in West pacific continent-ocean connection zone. *Earth Sci. Front.* 24, 152–170. doi:10.13745/j.esf.yx.2017-3-24

Kastowo, Leo, G. W., Gafoer, S., and Amin, T. C. (1996). *Geological map of the Padang quadrangle, Sumatera*. Bandung: Pusat Penelitian dan Pengembangan Geologi.

Koulakov, I., Kasatkina, E., Shapiro, N. M., Jaupart, C., Vasilevsky, A., Khrepy, S. E., et al. (2016). The feeder system of the Toba supervolcano from the slab to the shallow reservoir. *Nat. Commun.* 7, 12228. doi:10.1038/ncomms12228

McCarthy, A. J., and Elders, C. F. (1997). "Cenozoic deformation in Sumatra: Oblique subduction and the development of the Sumatran Fault system,"*Petroleum Geol. Southeast Asia*. Editors A. J. Fraser, S. J. Matthews, and R. W. Murphy (Geol. Soc. Spec. Pub.), 126, 355–363. doi:10.1144/GSL.SP.1997.126.01.21

Muksin, U., Bauer, K., Muzli, M., Ryberg, T., Nurdin, I., Masturiyono, M., et al. (2019). AcehSeis project provides insights into the detailed seismicity distribution and relation to fault structures in Central Aceh, Northern Sumatra. *J. Asian Earth Sci.* 171, 20–27. doi:10.1016/j.jseaes.2018.11.002

Nakano, M., Kumagai, H., Toda, S., Ando, R., Yamashina, T., Inoue, H., et al. (2010). Source model of an earthquake doublet that occurred in a pull-apart basin along the Sumatran fault, Indonesia. *Geophys. J. Int.* 181, 141–153. doi:10.1111/j.1365-246X.2010.04511.x

Natawidjaja, D. H., Bradley, K., Daryono, M. R., Aribowo, S., and Herrin, J. (2017). Late quaternary eruption of the Ranau caldera and new geological slip rates of the Sumatran Fault zone in southern Sumatra, Indonesia. *Geosci. Lett.* 4 (1), 21. doi:10.1186/s40562-017-0087-2

Nishimura, S., Abe, E., Nishida, J., Yokoyama, T., Dharma, A., Hehanussa, P., et al. (1984). A gravity and volcanostratigraphic interpretation of the Lake Toba region, North Sumatra, Indonesia. *Tectonophysics* 109, 253–272. doi:10.1016/0040-1951(84)90144-6

Nurfiani, D., Wang, X., Gunawan, H., Triastuty, H., Hidayat, D., Wei, S. J., et al. (2021). Combining petrology and seismology to unravel the plumbing system of a typical arc volcano: An example from Marapi, West Sumatra, Indonesia. *Geochem. Geophys. Geosyst.* 22, e2020GC009524. doi:10.1029/2020GC009524

Posavec, M., Taylor, D., Leeuwen, T. V., and Spector, A. (1973). Tectonic controls of volcanism and complex movements along the Sumatran Fault System. *Geol. Soc. Malay.* 6, 43–60. doi:10.7186/bgsm06197305

Prawirodirdjo, L., Bock, Y., Genrich, J. F., Puntodewo, S. S. O., Rais, J., Subarya, C., et al. (2000). One century of tectonic deformation along the Sumatran fault from triangulation and Global Positioning System surveys. *J. Geophys. Res.* 105, 28343–28361. doi:10.1029/2000jb900150

Pribadi, A., Mulyadi, E., and Pratomo, I. (2007). Mekanisme erupsi ignimbrit kaldera Maninjau, sumatera barat. *J. Geol. Indo.* 2, 31–41. (in Indonesian with English abstract). doi:10.17014/ijog.2.1.31-41

Purbo-Hadiwidjoyo, M. M., Sjachrudin, M. L., and Suparka, S. (1979). the volcano-Tectonic history of the Maninjau caldera, western Sumatra, Indonesia. *Geol. Mijnb.* 58, 193–200.

Salman, R., Lindsey, E. O., Feng, L., Bradley, K., Wei, S., Wang, T., et al. (2020). Structural controls on rupture extent of recent Sumatran Fault zone earthquakes, Indonesia. *J. Geophys. Res. Solid Earth.* 125, e2019JB018101. doi:10.1029/2019JB018101

Setiawan, I., Takahashi, R., and Imai, A. (2017). Petrochemistry of granitoids in sibolga and its surrounding areas, north Sumatra, Indonesia. *Resour. Geol.* 3, 254–278. doi:10.1111/rge.12132

Sieh, K., and Natawidjaja, D. H. (2000). Neotectonics of the Sumatran Fault, Indonesia. *J. Geophys. Res.* 105, 28, 295–28, 326. doi:10.1029/2000JB900120

Silitonga, P. H., and Kastowo (1995). *Geological map of the Solok quadrangle, sumatera*. Bandung: Pusat Penelitian dan Pengembangan Geologi.

Smithsonian Institution (2022). Global volcanism program. Availabile At: https://volcano.si.edu (Accessed July 29, 2022).

Stankiewicz, J., Ryberg, T., Haberland, C., Fauziand Natawidjaja, D. (2010). Lake Toba volcano magma chamber imaged by ambient seismic noise tomography. *Geophys. Res. Lett.* 37, L17306. doi:10.1029/2010GL044211

Suhendro, I. (2021). *The origin of transparent and nontransparent white pumice: A case study of the 52 ka Maninjau caldera-forming eruption, Indonesia*. Fukuoka, Japan: Kyushu University (Dissertation).

Tong, X., Sandwell, D. T., and Schmidt, D. A. (2018). Surface creep rate and moment accumulation rate along the Aceh segment of the Sumatran fault from L-band ALOS-1/PALSAR-1 observations. *Geophys. Res. Lett.* 45, 3404–3412. doi:10.1002/2017GL076723

Weller, O., Lange, D., Tilmann, F., Natawidjaja, D., Rietbrock, A., Collings, R., et al. (2012). The structure of the Sumatran Fault revealed by local seismicity. *Geophys. Res. Lett.* 39, L01306. doi:10.1029/2011GL050440

Wesnousky, S. (1988). Seismological and structural evolution of strike-slip faults. *Nature* 335, 340–343. doi:10.1038/335340a0

Wills, K., Daryono, M. R., Praet, N., Santoso, A. B., Dianto, A., Schmidt, S., et al. (2021). The sediments of Lake Singkarak and Lake Maninjau in West Sumatra reveal their earthquake, volcanic and rainfall history. *Sediment. Geol.* 416, 105863. doi:10.1016/j.sedgeo.2021.105863

Wilson, L., Sparks, R. S. J., and Walker, G. P. L. (1980). Explosive volcanic eruptions - IV. The control of magma properties and conduit geometry on eruption column behaviour. *Geophys. J. Int.* 63, 117–148. doi:10.1111/j.1365-246X.1980.tb02613.x

Zubaidah, T., Korte, M., Mandea, M., and Hamoudi, M. (2014). New insights into regional tectonics of the Sunda–Banda Arcs region from integrated magnetic and gravity modelling. *J. Asian Earth Sci.* 80, 172–184. doi:10.1016/j.jseaes.2013.11.013